JOURNAL OF SPACECRAFT AND ROCKETS
Vol. 45, No. 6, November–December 2008

Nonequilibrium Stagnation-Line Radiative Heating for Fire II

Christopher O. Johnston* and Brian R. Hollis†
NASA Langley Research Center, Hampton, Virginia 23681
and
Kenneth Sutton‡
National Institute of Aerospace, Hampton, Virginia 24060

DOI: 10.2514/1.33008

This paper presents a detailed analysis of the shock-layer radiative heating to the Fire II vehicle using a new air-radiation model and a viscous shock-layer flowfield model. This new air-radiation model contains the most up-to-date properties for modeling the atomic-line, atomic photoionization, molecular band, and non-Boltzmann processes. The applied viscous shock-layer flowfield analysis contains the same thermophysical properties and nonequilibrium models as the LAURA Navier–Stokes code. Radiation–flowfield coupling, or radiation cooling, is accounted for in detail in this study. It is shown to reduce the radiative heating by about 30% for the peak radiative heating points, although reducing the convective heating only slightly. A detailed review of past Fire II radiative heating studies is presented. It is observed that the scatter in the radiation predicted by these past studies is mostly a result of the different flowfield chemistry models and the treatment of the electronic state populations. The present predictions provide, on average throughout the trajectory, a better comparison with Fire II flight data than any previous study. The magnitude of the vacuum ultraviolet contribution to the radiative flux is estimated from the calorimeter measurements. This is achieved using the radiometer measurements and the predicted convective heating. The vacuum ultraviolet radiation predicted by the present model agrees well with the vacuum ultraviolet contribution inferred from the Fire II calorimeter measurement, although only when radiation–flowfield coupling is accounted for.

Nomenclature

$h\nu$	=	frequency, eV
I_w	=	wall-directed frequency-integrated radiative intensity, W/cm^2/sr
I_{w,h_ν}	=	wall-directed frequency-dependent radiative intensity, W/cm^2/sr/eV
j_ν	=	frequency-dependent emission coefficient, erg/cm^3/sr
q_c	=	convective heat flux, W/cm^2
q_r^-	=	wall-directed radiative heat flux, W/cm^2
$q_{r,h\nu}^-$	=	wall-directed frequency-dependent radiative heat flux, W/cm^2/eV
q_{total}	=	total heat flux absorbed by the Fire II calorimeter, equal to $q_c + \alpha q_r^-$, W/cm^2
t	=	time, s
T_{ve}	=	vibrational-electronic-electron temperature, K
T_{tr}	=	translational-rotational temperature, K
z	=	distance along the stagnation line measured from the wall, cm
αq_r^-	=	radiative flux absorbed by the beryllium calorimeter, W/cm^2

Subscripts

$h\nu$	=	spectral dependence in terms of electron volts
inferred	=	value obtained from the combination of a measurement and prediction

Superscripts

nc	=	a noncatalytic wall boundary condition was applied
sc	=	a supercatalytic wall boundary condition was applied
$-$	=	radiative flux or intensity directed toward the vehicle wall

Presented as Paper 3908 at the 10th AIAA/ASME Joint Thermophyics Conference, Miami, FL, 25–28 June 2007; received 22 June 2007; revision received 21 April 2008; accepted for publication 28 April 2008.

*Aerospace Engineer. Member AIAA.
†Aerospace Engineer. Senior Member AIAA.
‡Senior Research Fellow. Associate Fellow AIAA.

I. Introduction

THE heat flux to a vehicle at lunar-return conditions consists of a component due to the radiative flux from the high-temperature shock-layer gas [1]. The prediction of this radiative flux has been studied sporadically since the beginning of manned space flight, with significant progress being made for NASA's Apollo program. In support of this research, the Fire II flight experiment obtained radiative heating measurements at conditions similar to those for lunar return [2,3]. These measurements have since become a benchmark for new radiative heating prediction algorithms. The goal of this paper is to review the past predictions of these data and to present the results of a newly developed air-radiation model, which was presented recently by Johnston et al. [4,5]. These results have been updated since the previous publication of this work [6], which was based on an earlier version [7] of the developed radiation model.

A review of past studies of the Fire II radiative heating is presented in Sec. II. The various predictions to the flight data are compared and the differences discussed. The flowfield and radiation model used by each researcher is defined, and its influence on the comparison with the flight data is assessed. The viscous shock-layer (VSL) flowfield model used in the present study is discussed in Sec. III. A brief description of the radiation model applied in the present study is presented in Sec. IV. The Fire II radiative and convective heating predicted using the present flowfield and radiation models are presented in Sec. V for the case where radiation–flowfield coupling is not considered. These results, which are known to be physically inaccurate, are presented to provide a baseline for comparing with the radiation–flowfield coupled cases. Sec. VI compares the radiation–flowfield coupled results of the present study with the flight data and various past predictions. The deviations of the present results from the flight data and previous studies are discussed, and the influence of non-Boltzmann radiation and flowfield coupling are shown. The

differences between the radiation predicted by a two-temperature chemical nonequilibrium VSL flowfield and a single-temperature chemical equilibrium VSL flowfield are compared, which provides insight into the effect of multiple temperatures and chemical nonequilibrium on the radiative heating predictions and the effect of radiation–flowfield coupling.

II. Review of Past Studies

The Fire II flight experiment was flown in 1965 to obtain radiative heating data for a capsule with a scaled-down Apollo-shaped forebody [2]. Three nonablating beryllium heat shields were attached to the vehicle, with the first two being jettisoned at selected points in the trajectory. Table 1 lists the flight conditions and wall temperature at various trajectory points along with the vehicle nose radius, which is different for the various heat shields. Radiative heating data were obtained in the stagnation region with three different types of instrumentation. A *total* radiometer measured the radiative intensity behind a quartz window, which allowed the radiation in the spectral range of 0–6 eV to be measured. A *spectral* radiometer provided spectrally-resolved intensity data in the spectral range of 2.2–4.1 eV with a resolution of about 0.04 eV and a reported uncertainty of ±23%. A beryllium calorimeter measured the convective heating plus the *absorbed* radiative flux. The *absorbed* radiative flux refers to the component that is absorbed by the beryllium calorimeter over the entire spectrum. The spectral absorptance of beryllium is reported by Cornette [3].

Many researchers have used the Fire II case as a benchmark for a new radiation code or flowfield solver [8–17]. Table 2 lists those studies published since 1984, which are the most relevant to modern studies. Listed along with each researcher are the flowfield equations, chemistry model, radiation code, and method of obtaining the molecular and atomic state populations implemented in the particular study. All of the studies listed here include radiation–flowfield coupling, meaning the divergence of the radiative flux is included in the energy equation.

The most widely analyzed data from the three measuring devices are the total radiometer data, which was presented in Fig. 13 of Cauchon [2] as the radiative intensity integrated between 0 and 6 eV. Figure 1 compares the intensity values predicted by many of the researchers listed in Table 2 with the flight data. According to Cauchon, the total radiometer data contains an uncertainty of ±20%, which is indicated by the error bars in the figure. The results of Olynick et al. [16] compare best with the data, whereas the results of Gupta [10] are also in good agreement throughout the trajectory. From Table 2, it is seen that Olynick et al. [16] applied the code NOVAR, which assumed a Boltzmann distribution of electronic states, to a Navier–Stokes nonequilibrium flowfield. The NOVAR code is reported to be essentially the same as LORAN, except that it is configured for computational efficiency and assumes a Boltzmann distribution of electronic states, instead of applying the non-Boltzmann quasi-steady-state (QSS) model used in LORAN and NEQAIR. Note that the results of Olynick et al. compare well for the early trajectory points. This is unexpected because a large percentage of the shock layer is in nonequilibrium for these points, which should have caused the Boltzmann assumption to over-predict the radiation considerably [15]. In addition to the Boltzmann results, Olynick et al. [16] also presented several cases that applied the non-Boltzmann QSS model. These results showed that the QSS and Boltzmann models agreed for the early nonequilibrium trajectory points and then diverged from each other for the later equilibrium points. This trend is inconsistent with other studies [18], which show that a Boltzmann distribution of electronic states is approached in regions of chemical equilibrium.

Another interesting feature of Fig. 1 is the good agreement with the data obtained by Gupta [10], who applied the RAD/EQUIL code to an equilibrium VSL flowfield. In a similar study, Sutton [8] also applied the RAD/EQUIL code to an equilibrium flowfield, although it was inviscid. Assuming that similar thermodynamic properties were used and that the radiation codes applied were actually the same, it would be expected that because of boundary layer absorption, Gupta's [10] values should be slightly lower than Sutton's [8]. Surprisingly, Fig. 1 shows the opposite trend throughout the trajectory. Furthermore, the results of Balakrishnan et al. [9] should agree very well with Gupta's [10], because they both applied the RAD/EQUIL code to an equilibrium VSL flowfield (although their VSL techniques were different). It is seen in Fig. 1 that the results of Gupta [10] and Balakrishnan et al. [9] do not compare well. Unlike Gupta's [10] values, the values of Balakrishnan et al. [9] are lower than Sutton's [8] inviscid results,

Table 1 Trajectory points for Fire II cases

t, s	Altitude, km	Density, kg/m^3	Velocity, km/s	Temperature, K	Wall temperature, K	Physical R_N, m
1634.0	76.42	3.72×10^{-5}	11.36	195	615	0.935
1636.0	71.02	8.57×10^{-5}	11.31	210	810	0.935
1637.0	67.05	1.47×10^{-4}	11.25	228	1030	0.935
1640.0	59.62	3.86×10^{-4}	10.97	254	1560	0.935
1643.0	53.04	7.80×10^{-4}	10.48	276	640	0.805
1645.0	48.37	1.32×10^{-3}	9.83	285	1520	0.805
1648.0	41.60	3.25×10^{-3}	8.10	267	503	0.702

Table 2 Summary of previous Fire II studies

Researcher	Reference	Flowfield equations[a]	Chemistry[b]	Radiation code	State populations[c]
Sutton (1984)	[8]	Euler	E	RAD/EQUIL	B
Balakrishnan et al. (1985)	[9]	VSL	E	RAD/EQUIL	B
Gupta (1987)	[10]	VSL	E	RAD/EQUIL	B
Bird (1987)	[11]	DSMC	NE	custom	NB
Carslon (1989)	[12]	VSL	E	8-step model	NB
Park (1989)	[13]	VSL	NE	NEQAIR85	NB
Gally (1992)	[14]	VSL	NE	RAD/EQUIL	NB
Greendyke et al. (1994)	[15]	NS	NE	LORAN	NB
Olynick et al. (1994)	[16]	NS	NE	NOVAR	B
Park (2004)	[17]	VSL	NE	NEQAIR04	NB

[a]VSL is the viscous shock er, DSMC is direct simulation Monte Carlo, NS is Navier–Stokes.
[b]E is equilibrium, NE is nonequilibrium.
[c]B is Boltzmann, NB is non-Boltzmann.

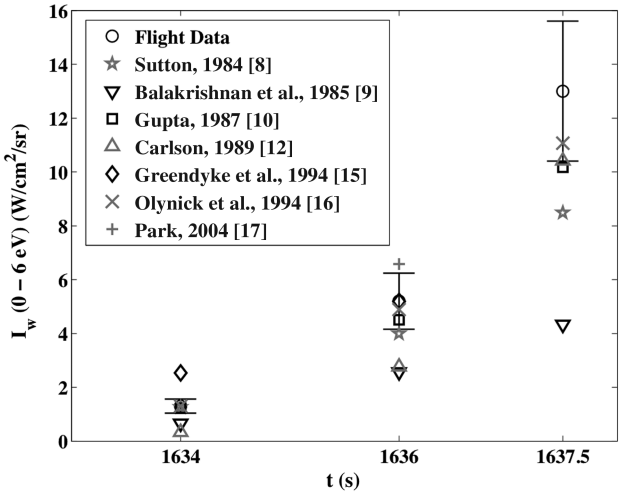

a) Early trajectory points

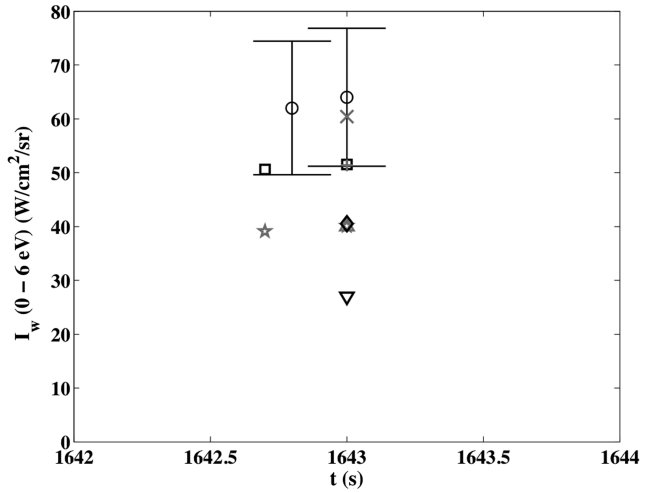

b) Peak heating trajectory points

Fig. 1 Comparison of past predictions with the Fire II total radiometer data for the partial intensity at the wall.

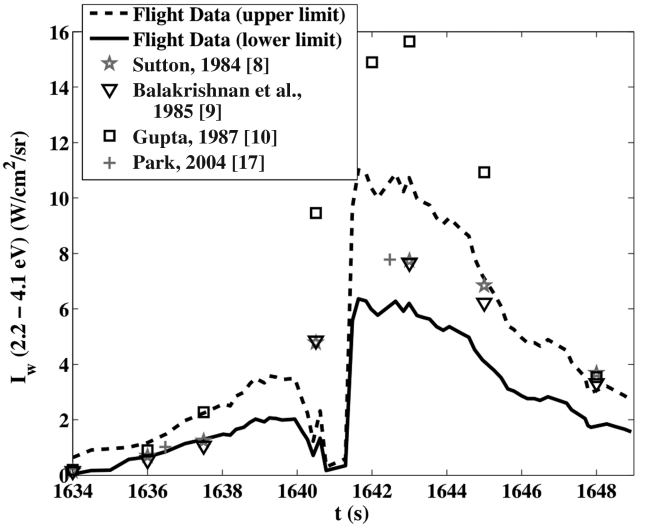

Fig. 2 Comparison of past predictions with the frequency-integrated Fire II spectral radiometer data.

which indicate the expected influence of boundary layer absorption. It is possible (although it is not stated) that Gupta [10] included RAD/EQUIL's optional negative nitrogen ion contribution, which was not applied by Sutton [8] or Balakrishnan et al. [9] and would increase the emission in the 0–6-eV range [4].

The most state-of-the-art studies presented in Fig. 1 are those of Greendyke and Hartung [15] and Park [17], which both applied a nonequilibrium radiation model to a coupled thermochemical nonequilibrium flowfield. Although these studies agree reasonably well with the data, they do not significantly improve upon the results of older studies. A reason for this lack of improvement, especially for the early trajectory points, is the uncertainty in the nonequilibrium flowfield modeling (which was not an issue with the older chemical equilibrium studies). This point is made clear in a study by Hartung et al. [19], who adjusted some of the unknown nonequilibrium flowfield parameters and studied their effect on the radiative heating for the Fire 1631, 1634, and 1637.5 s cases. It was shown that the integrated intensity between 0 and 6 eV varied for the 1634 and 1637.5-s cases between 1.8–4.4 and 11.0–20.0 W/cm^2-sr, respectively, depending upon the nonequilibrium flowfield parameters chosen. Although recommended values for the parameters are provided in the literature [20–22], the evidence supporting these values is not overwhelming.

The frequency-integrated data from the spectral radiometer (between 2.2 and 4.1 eV), presented in Fig. 13 of Cauchon [2], has been the subject of comparison by only a few researchers. The comparison between the data and predictions are shown in Fig. 2. The two flight data lines represent the upper and lower limits of the data scatter. The predictions all agree reasonably well, although none of them stay within the data scatter throughout the entire trajectory. An interesting aspect of this comparison is the close agreement of the values predicted by Sutton [8] and Balakrishnan et al. [9], as opposed to Fig. 1 where the two differ significantly, especially near the peak heating point. A few studies also compared their predictions with the *spectrally-resolved* data [23] from the spectral radiometer [17,19]. Park [17] showed that his predicted spectrum compared well with the measured spectrum for the 1643 s point. This result is consistent with the good comparison of the frequency-integrated values presented in Fig. 2. Hartung et al. [19] compared their computed spectra obtained with the LORAN code with the data for the 1631, 1634, and 1637.5 s trajectory points. The agreement with the data for these nonequilibrium cases was not very good, but because they did not present values for the integrated intensity between 2.2 and 4.1 eV, it is difficult to quantify the disagreement. From Fig. 5 of Hartung [24] and Figs. 6–7 presented by Greendyke [25], it is suspected that the non-Boltzmann modeling of N_2 and N_2^+ are likely responsible for this poor agreement with the data. The 2.2–4.1-eV region of the spectrum is dominated by the $N_2(1^+)$ and $N_2^+(1^-)$ bands, which emit strongly in the nonequilibrium region near the shock. The LORAN code applied by Hartung uses the same non-Boltzmann QSS model as NEQAIR.

The Fire II calorimeter data presented by Cornette [3] provide heating values that contain the convective heating plus the contribution of the radiative flux absorbed by the beryllium calorimeter. A comparison of the calorimeter data with various predictions throughout the trajectory is presented in Fig. 3. The $\pm 5\%$ error bars on the data in this figure indicate the measurement uncertainty according to Cornette. Although the flight data cannot be separated into convective and radiative components, Fig. 4 compares the calculated values of these components, whose values add together to produce the values shown in Fig. 3. The best comparisons with the data in Fig. 3 are the results of Olynick et al. [16], as was the case for the radiometer data in Fig. 1. It is also seen in Fig. 3 that the results of Sutton [8] and Gupta [10] are in close agreement with each other throughout the trajectory. This agreement is due to their offsetting differences in the radiative and convective components. Surprisingly, Sutton's [8] radiative component is larger than Gupta's [10], which is the opposite of what was seen in Fig. 1 for the 0–6 eV integrated intensity. This indicates that Sutton predicted a larger radiative contribution from the spectral region above 6 eV (the vacuum ultraviolet, or VUV) than Gupta. This difference is likely due to boundary layer absorption present in Gupta's case (and not in Sutton's [8]), which decreases the VUV component (although barely influencing the 0–6-eV component). The results of Greendyke and Hartung [15] disagree significantly with the data. It is seen that both

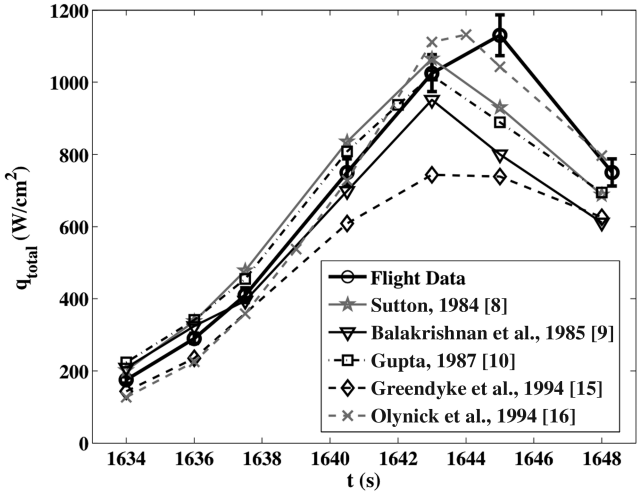

Fig. 3 Comparison of past predictions for the total absorbed heat flux with the Fire II calorimeter data.

the convective and radiative predictions are too low, especially near peak heating. Note that the large difference in convective heating predicted by Greendyke and Hartung [15] and Olynick et al. [16] is present even though both studies applied a nonequilibrium Navier–Stokes flowfield with a supercatalytic wall boundary condition.

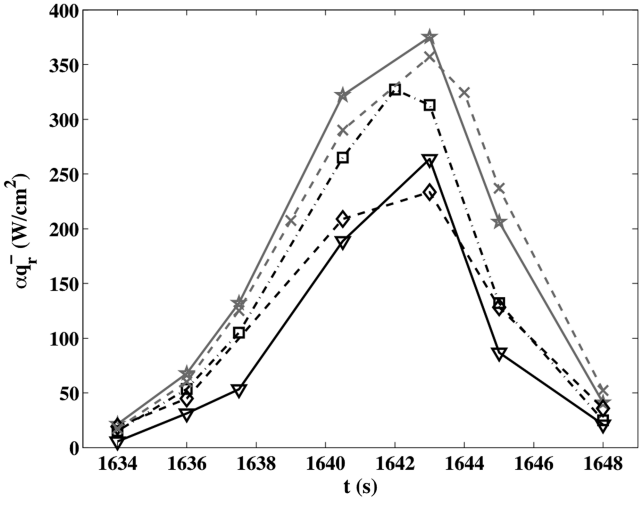

a) Radiation absorbed by the calorimeter (αq_r^-)

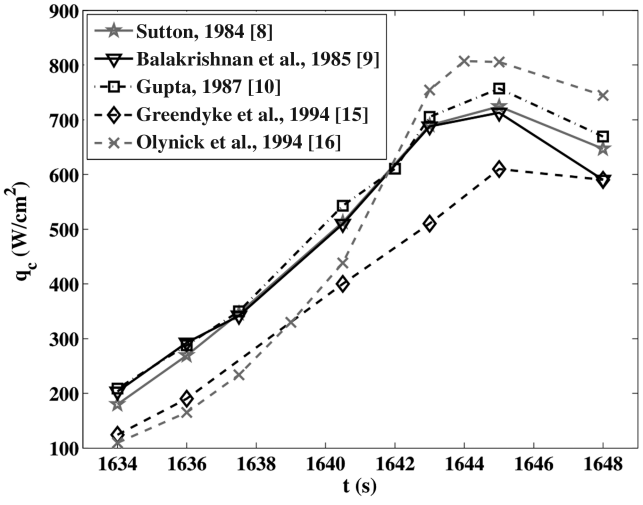

b) Convective heating (q_c)

Fig. 4 Predictions by various researchers for the two components of the calorimeter measurement.

III. Flowfield Model

The flowfield and radiation model applied in the present study is discussed in detail by Johnston [7]. A VSL method [26] was applied for the flowfield model. This method allows for a computationally efficient solution that retains all of the important flowfield physics for the stagnation region of a blunt body. Only the stagnation-line flowfield was considered in the present study, although the same method may be used to obtain solutions downstream of the stagnation line. The same kinetic models and thermophysical properties are applied in the present VSL code as are applied in the LAURA code [27]. The air model applied consists of the following 11-species: N_2, N_2^+, O_2, O_2^+, NO, NO^+, N, N^+, O, O^+, and e^-. The forward chemical rates were taken from Park [28], whereas the backward rates were obtained by applying detailed balancing, with the equilibrium constants calculated using curve fits from McBride et al. [29]. These curve fits were also used to calculate the specific heat and enthalpy values for each species. The collision cross sections required for the calculation of the diffusion, viscosity, and thermal conductivity coefficients were taken from Gupta et al. [30]. Multicomponent diffusion was modeled using the "approximate-corrected" approach presented by Sutton and Gnoffo [31].

To validate the developed VSL model for lunar return conditions, comparisons were made with Navier–Stokes results produced by the LAURA code for Fire II cases. The temperature and species number densities (relevant to the radiation calculation) predicted by the VSL method and the LAURA code are compared in Fig. 5 for the Fire II 1636 s trajectory point. This point was chosen because the shock layer contains both a region of chemical equilibrium and nonequilibrium. In these figures, the vehicle wall is located at $z = 0$, where z is the distance along the stagnation line. The consequence of the different treatments of the bow shock wave by the two methods is clearly shown in these figures. The "discrete shock" model of the VSL approach is seen to result in a larger translational-rotational temperature directly behind the shock, even with the application of the shock-slip equations. Along with beginning at a higher temperature directly behind the shock, the T_{tr} values in Fig. 5a are seen to behave slightly different in the nonequilibrium region directly behind the shock. This is another consequence of the discrete shock treatment, which results from T_{tr} beginning its relaxation process behind the shock at a higher temperature than for the LAURA case. The T_{ve} values, on the other hand, are in relatively good agreement in the nonequilibrium regions. This is fortunate because T_{ve} governs the radiation. Other than the differences near the shock, the temperature profiles shown in Fig. 5a closely agree throughout the rest of the shock er. The locations at which the two temperatures equilibrate compare well between the methods, as do the values of the temperatures in the equilibrium regions of the layer, which agree within 1% for this case. This close agreement in the equilibrium region of the shock layer is required for the prediction of similar radiative emission values, because of the exponential T_{ve} dependence of the radiative emission. This exponential dependence is due to the Boltzmann distribution of the upper electronic state of the various radiative transitions, and hence is only true in the regions of chemical equilibrium where a Boltzmann distribution is approached. Conversely to this exponential dependence on temperature, *most* of the radiative emission depends linearly on the species number densities (the atomic bound-free emission has essentially a quadratic dependence). The disagreement in the equilibrium regions of no more than 5% for the present model is therefore regarded as sufficient. It is shown in [7] that the radiative flux resulting from the present VSL flowfield and the LAURA flowfield, applying the same radiation model, agree within 5% at the wall.

IV. Radiation Model

The radiation model applied in the present study is discussed in detail by Johnston et al. [4,5], which has been updated since the previous version of this work was published [6]. The results

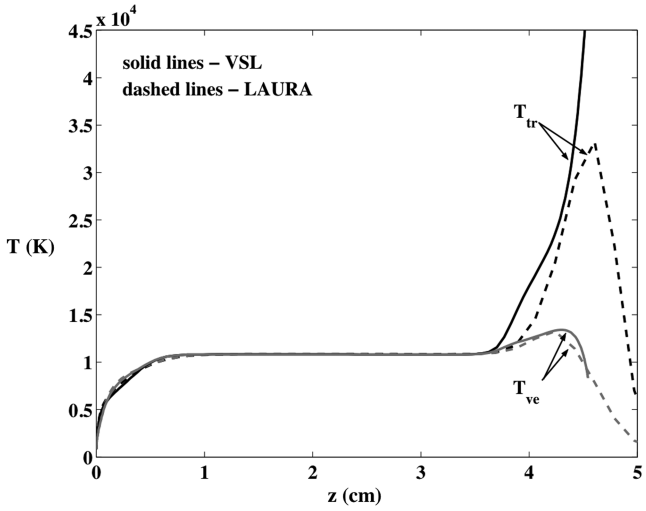

a) Temperature profiles

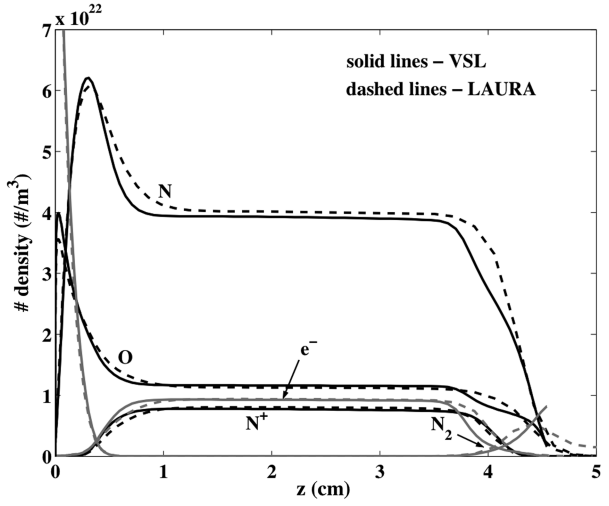

b) Number densities

Fig. 5 Comparison of the VSL and LAURA stagnation-line flowfields for the Fire-1636 case.

presented throughout this paper have been updated accordingly, although the differences are minor and do not change any conclusions. The updated model is based on a set of atomic levels and lines obtained from the National Institute of Standards and Technology (NIST) online database [32] and the Opacity Project [33], as well as atomic bound-free cross sections from the TOPbase [34]. The negative nitrogen and oxygen ions are treated using cross sections suggested by Soon and Kunc [35] and Chauveau et al. [36], respectively. The molecular band systems are treated using a smeared-rotational band (SRB) model [37], which was shown by Johnston et al. [4] to be accurate, at the present flowfield conditions, for treating strongly absorbing and emitting band systems. The molecular data for modeling these band systems are obtained from Laux [38], except for the VUV N_2 systems, which are obtained from various other sources [39–41]. The non-Boltzmann modeling of the atomic and molecular electronic states is based on a set of electron-impact excitation rates compiled from the literature and presented in detail by Johnston [7]. Following the work of Park [42], the quasi-steady state assumption is made when solving the master equation. The tangent-slab approximation is applied to calculate radiative flux and the divergence of the radiative flux, which is required for the radiation–flowfield coupling procedure. Comparisons between this radiation model and RAD/EQUIL are presented in [4], where it is shown that the present model predicts roughly 15% larger emission values from the 0–6-eV range, and similar values in the 6–16-eV range.

V. Uncoupled Radiative Heating for Fire II

The Fire II flight experiment was discussed in detail in Sec. II. Along with presenting the flight data, it was shown in this section that there is a large scatter among the previous theoretical predictions of this data. Furthermore, no prediction method compared well throughout both the early nonequilibrium region of the trajectory and in the later mostly equilibrium peak-heating region. It was shown that the more recent and sophisticated prediction methods did not lead to a consistently better comparison with the data relative to older prediction methods. The goal of this section and Sec. VI is to compare the results of the new flowfield and radiation models presented in Secs. III and IV with the flight data and previous predictions. Although the uncoupled results are known to be physically inaccurate, they are presented in this section so that they may be compared with the uncoupled values predicted by previous studies. This allows the differences in the flowfield and radiation models to be examined without the complication of radiation–flowfield coupling. Furthermore, it will be insightful to compare these uncoupled values with the coupled values presented in the next section.

The chemical kinetics and thermophysical properties applied in the present flowfield model were discussed in Sec. III. Examples of uncoupled Fire II flowfields were also presented in that section and shown to provide uncoupled radiative heating values consistent with those resulting from a LAURA (Navier–Stokes) flowfield. Table 3 lists the various radiative components predicted with the present *uncoupled* nonequilibrium VSL and radiation models discussed in Secs. III and IV. The q_r^- and I_w values listed here represent the wall-directed radiative flux and wall-directed intensity, respectively, at the wall ($z = 0$). The numbers in parentheses in the header column represent the spectral range, in electron volts, included in each value. The αq_r^- values represent the radiation absorbed by the beryllium calorimeter, which is a quantity required for comparison with the calorimeter data (as mentioned previously in the discussion of Fig. 4). Also required for the comparison with the calorimeter data is the convective heating q_c, which is listed in this table assuming both a supercatalytic (sc) and noncatalytic (nc) wall. The difference in the radiation predicted by these two catalyticity assumptions is negligible, and so only the results from the supercatalytic case are presented.

The two previous studies that present uncoupled results over the majority of the trajectory are the studies by Olynick et al. [16] and Greendyke and Hartung [15]. The comparison between the q_r^- and $I_w(0–6)$ values presented in Table 3 and those presented in Table 5 of Olynick et al. [16] indicates agreement within 10% over most of the trajectory. The values presented by Greendyke and Hartung [15] in their Figs. 4 and 5, on the other hand, are lower than the present values by up to 30%. The fact that Olynick et al. [16] values agree well, whereas Greendyke and Hartung's [15] do not, is interesting considering that Olynick et al. [16] applied a Boltzmann model and Greendyke and Hartung [15] applied a non-Boltzmann model for the electronic state populations. As mentioned previously, the present study also applies a non-Boltzmann model, which is known to result in less radiation than the Boltzmann model, especially in regions of significant chemical nonequilibrium. Note that the flowfields predicted by Greendyke and Hartung [15] and Olynick et al. [16] were significantly different (see Fig. 3 of Olynick et al.), even though both were nonequilibrium Navier–Stokes solutions.

After the completion of the present research, the study by Hash et al. [43] of the uncoupled convective and radiative heating for Fire II became available to the authors. This work compared the convective heating predicted by various state-of-the-art Navier–Stokes codes. Because the present flowfield model applies the same energy equation and thermophysical modeling as the LAURA code, the LAURA results presented by Hash et al. should compare well with the present results. The supercatalytic and noncatalytic convective heating predicted by the LAURA code at 1636 s agree with the present results within 2%. For the 1643-s case, the supercatalytic value agrees within 3% and the noncatalytic value agrees within 9%. The current radiation results are 32% greater in the

Table 3 Uncoupled convective and radiative heat flux values (W/cm^2) and radiative intensities ($W/cm^2/sr$) for the Fire II vehicle obtained using the NE VSL flowfield model

t, s	q_c sc	q_c nc	αq_r^-(0–18)	αq_r^-(0–6)	αq_r^-(6–18)	q_r^-(0–18)	q_r^-(0–6)	q_r^-(6–18)	I_w (0–18)	I_w (0–6)	I_w (6–18)
1634.0	221	115	23.0	6.70	16.3	31.3	13.3	18.0	6.28	2.17	4.11
1636.0	316	195	77.9	20.4	57.5	106	42.4	63.3	22.2	7.16	15.0
1637.5	398	266	157	42.0	115	217	89.5	127	46.6	15.4	31.2
1640.5	578	439	416	135	281	609	293	316	133	52.0	81.3
1643.0	777	689	464	179	285	713	389	324	153	69.4	83.9
1645.0	835	743	220	107	113	354	227	130	73.6	40.5	33.1
1648.3	756	670	29.3	18.7	10.6	51.4	36.1	15.3	8.73	5.95	2.78

Table 4 Coupled convective and radiative heat flux values (W/cm^2) and radiative intensities ($W/cm^2/sr$) for the Fire II vehicle obtained using the NE VSL flowfield model

t, s	q_c sc	q_c nc	αq_r^-(0–18)	αq_r^-(0–6)	αq_r^-(6–18)	q_r^-(0–18)	q_r^-(0–6)	q_r^-(6–18)	I_w (0–18)	I_w (0–6)	I_w (6–18)
1634.0	217	111	19.7	6.33	13.4	27.2	12.4	14.8	5.42	2.02	3.40
1636.0	308	188	62.4	18.0	44.4	86.1	37.1	48.9	17.9	6.24	11.7
1637.5	387	257	120	35.6	84.5	169	75.2	93.8	35.9	12.9	23.0
1640.5	563	428	296	106	190	445	230	215	95.9	40.7	55.2
1643.0	756	673	344	144	200	540	311	229	114	55.4	58.9
1645.0	817	731	184	93.6	90.4	303	198	105	61.8	35.3	26.4
1648.3	774	693	24.6	15.2	9.36	43.1	29.3	13.8	7.22	4.78	2.44

0–6-eV range and 51% greater in the 6–18-eV range than the NEQAIR results presented by Hash et al. for the 1636-s case.

VI. Coupled Radiative Heating for Fire II

The radiation components predicted by the present radiation-coupled flowfield model are presented in Table 4 for the Fire II case. The column definitions are identical to those of Table 3. To illustrate the differences between these values and the uncoupled results discussed previously, Fig. 6 compares q_c, q_r^-, and aq_r^- between the coupled and uncoupled cases. It is seen that the q_r^- and αq_r^- values are reduced by 20–30% throughout the main heating portion of the trajectory. This reduction is slightly larger than the 15–25% reduction reported by Olynick et al. [16] and the 5–18% reduction reported by Greendyke and Hartung [15]. The smaller reduction found by Greendyke and Hartung is most likely a result of their significantly smaller uncoupled radiation prediction, which reduces the coupling effect. The discrepancy with the result of Olynick et al. [16] is likely a result of differences in the flowfield modeling.

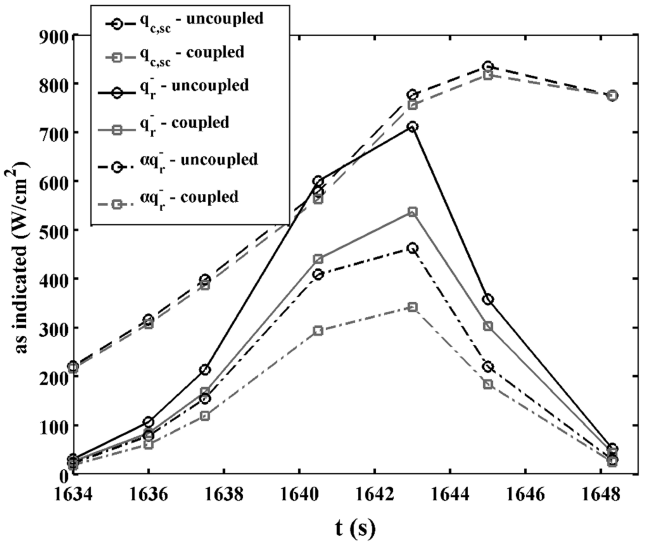

Fig. 6 Uncoupled and coupled values for the convective and radiative heat flux along the Fire II trajectory. The αq_r values represent the radiative flux absorbed by the calorimeter.

A significant difference between Olynick et al. flowfield model and the present model is that Olynick et al. obtains the vibrational-electronic-electron temperature by solving the vibrational energy equation, and *not* the vibrational-electronic-electron energy equation, as is done in the present model. The consequence of this treatment by Olynick et al. is that the divergence of the radiative flux does not appear in the vibrational energy equation, even though the temperature obtained from this equation governs the magnitude of the radiation. The influence of radiation on the behavior of the two temperatures is therefore fundamentally different for this model because radiation does not directly influence the vibrational-electronic-electron temperature. For the high-temperature shock layers of present interest, the vibrational energy is very small throughout most of the shock layer because the majority of the molecules are dissociated. Furthermore, the coupling of the vibrational energy mode to the translational energy mode is represented through vibrational-translational energy relaxation, which is shown in Eq. 55 of Gnoffo et al. [27] to be proportional to the mass fractions of the molecules. For the present highly-dissociated conditions, this term is small, which results in the vibrational energy mode being weakly coupled to the translational energy mode. This indicates the possible inadequacy in solving the vibrational energy equation instead of the vibrational-electronic-electron energy equation for the high-temperature shock layers of present interest.

The influence of radiation–flowfield coupling on a two-temperature chemical nonequilibrium flowfield should be similar to that predicted by a single-temperature chemical-equilibrium model, assuming that the electron-translational energy exchange term is properly treated (for the two-temperature model). By comparing the present two-temperature chemical nonequilibrium VSL flowfield (NE VSL) with a chemical equilibrium VSL flowfield (E VSL), the influence of coupling on the two models may be compared. Figure 7 compares the partial intensity (0–6 eV) at the wall predicted by the uncoupled and coupled NE VSL and E VSL predictions. The decrease in intensity with the addition of coupling is seen to be very similar for both flowfield models. This confirms the previous statement regarding the similarity of the coupling effect for the two flowfield models. Figure 8 presents the coupled and uncoupled temperature profiles for the NE VSL and E VSL models at the 1643-s condition. Note that the vertical axis of this figure ranges from 10,000–12,000 K, for clarity. Except for the differences in the boundary layer, which is a result of the different diffusion modeling and possible nonequilibrium effects, the NE VSL and E VSL models compare very well for both the coupled and uncoupled cases.

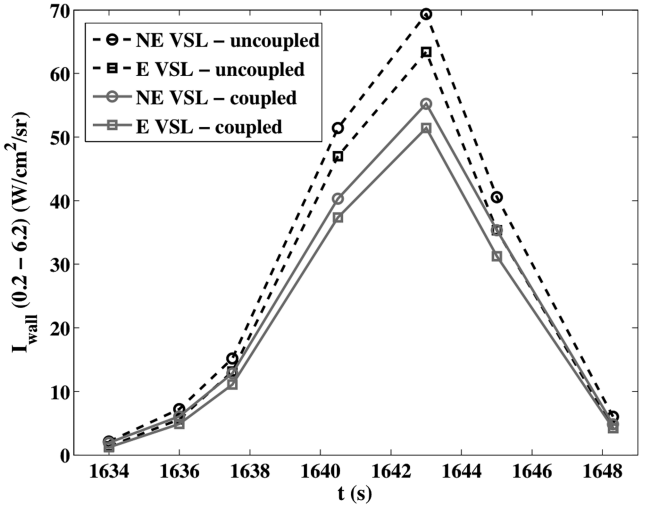

Fig. 7 Partial wall intensity values (0–6 eV) predicted by the coupled and uncoupled application of the NE and E VSL flowfield models.

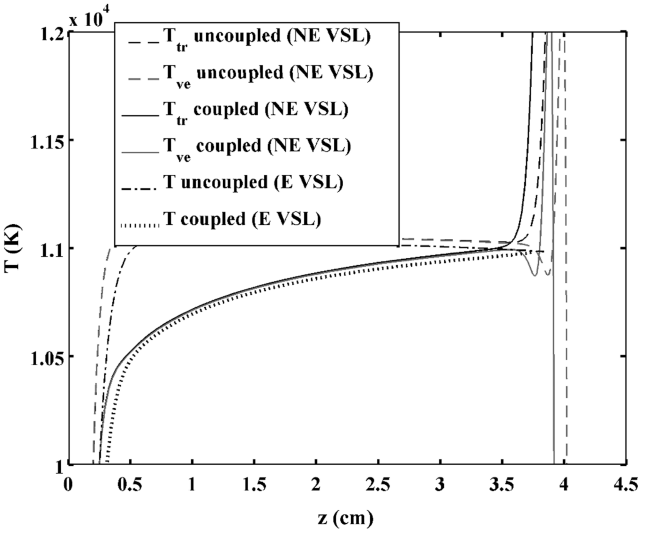

Fig. 8 Uncoupled and coupled stagnation-line temperature profiles for $t = 1643$ s.

The slight separation seen between the models throughout the layer is only 10–20 K, which is negligible relative to the temperatures of roughly 11,000 K.

To assess the influence of non-Boltzmann modeling and radiation–flowfield coupling on the radiative flux throughout the shock layer and on the flux that ultimately reaches the wall, Figs. 9 and 10 present the wall-directed spectrally-integrated radiative flux profiles through the shock layer and the radiative flux spectrum at the wall. In these figures, both the non-Boltzmann and Boltzmann results are presented for the uncoupled case, although only the non-Boltzmann result is presented for the coupled case. The non-Boltzmann and Boltzmann terminology used here specifies that the atomic *and* molecular electronic states are modeled by their respective Boltzmann or non-Boltzmann models. These models are discussed in detail by Johnston et al. [5,7]. The cumulative flux values presented in Figs. 9 and 10 allow for the contributions from the various radiative mechanisms to be compared (note that the *spectrum* for only the coupled non-Boltzmann case is presented in each figure). For the 1636-s case, the non-Boltzmann influence is seen to be large. This is a result of the relatively large region of nonequilibrium directly behind the shock, which was shown previously in Fig. 5. From Fig. 9b, the increased flux for the Boltzmann case is seen to come from the atomic lines between 1.3 and 1.8 eV and the N_2^+ first-negative band system located between 2

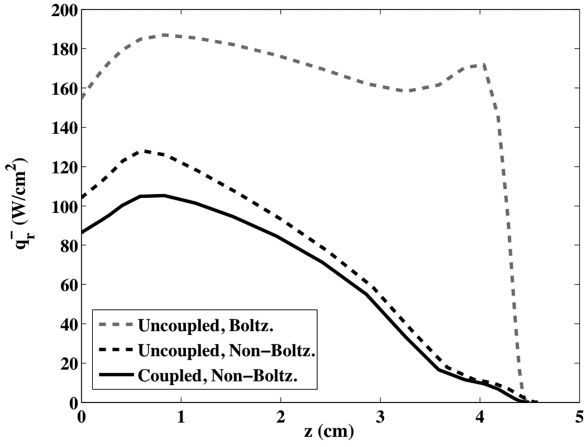

a) Wall-directed radiative flux profiles

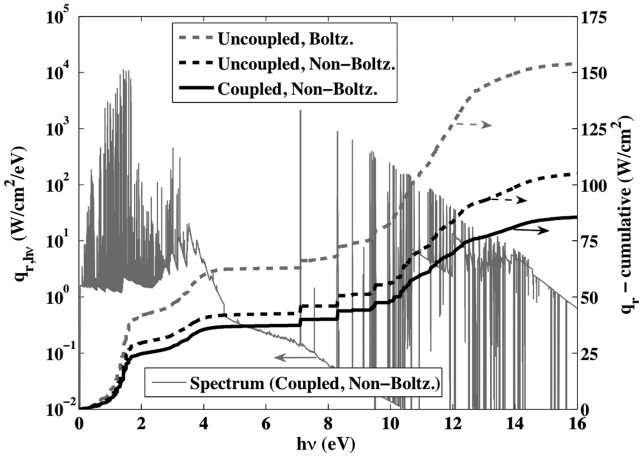

b) Wall spectrum and cumulative fluxes

Fig. 9 Coupled and uncoupled NE VSL predictions for $t = 1643$ s.

and 5 eV. The atomic bound-free continuum located above 12 eV also provides some excess radiation for the Boltzmann case. For the 1643-s case, Fig. 10 shows that the Boltzmann influence is small. This is a result of most of the shock layer being in equilibrium, which was shown by the temperature profiles presented in Fig. 8. The influence of coupling for both the 1636 and 1643-s cases is seen to result mostly from the atomic lines located between 1.3 and 1.8 eV and the atomic bound-free continuum located above 10 eV.

The Fire II total radiometer data and the theoretical predictions of this data by past studies were presented in Sec. II. The data are compared in Fig. 11 with the present radiation model coupled to the nonequilibrium (NE VSL) and equilibrium flowfield (E VSL) models. The predictions from past studies are also shown in these figures for comparison. Figure 11b focuses on the peak heating trajectory points, whereas Fig. 11a focuses on the three earliest points, which are important because they contain a significant amount of nonequilibrium radiation. From Fig. 11b the differences between the flight data, previous predictions, and the present predictions can clearly be seen for the 1643 s point. For this trajectory point, the study by Olynick et al. [16] is the only previous prediction that is closer to the data than the present NE VSL result. As discussed in this section, the Olynick et al. values are likely larger because of the reduced influence of radiation–flowfield coupling, resulting from the different treatment of the energy equations and temperatures. The Boltzmann assumption applied by Olynick et al. should not influence the radiation at 1643 s because the flowfield is mostly in equilibrium, as indicated in Fig. 10. Note that the present equilibrium values (E VSL) are slightly larger than the values predicted by Gupta [10], who also applied an E VSL method. Assuming that the flowfield models were nearly equivalent, this trend is consistent with the fact that the present radiation model predicts larger radiation values for a

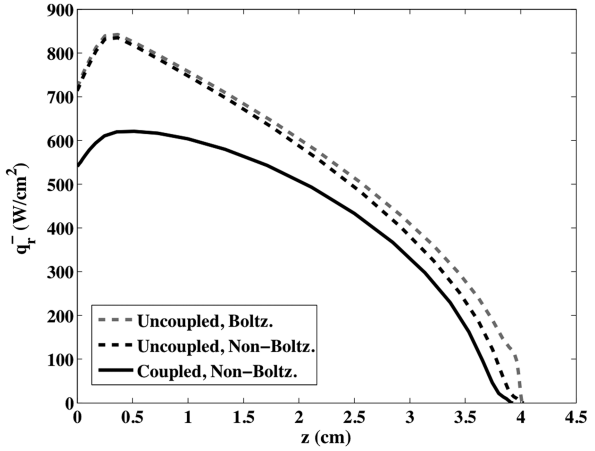

a) Wall-directed radiative flux profiles

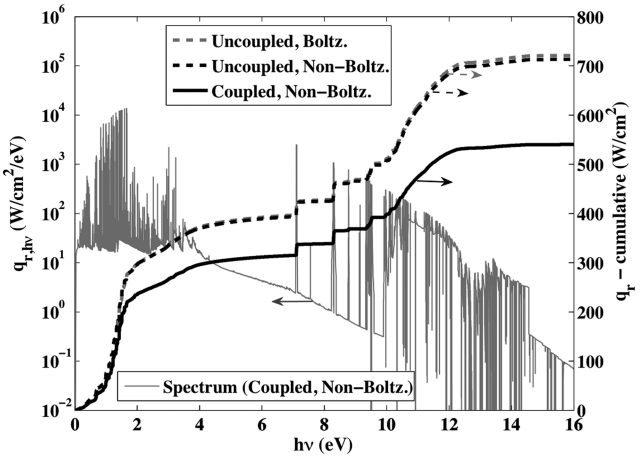

b) Wall spectrum and cumulative fluxes

Fig. 10 Coupled and uncoupled NE VSL predictions for $t = 1643$ s.

given condition than the RAD/EQUIL code applied by Gupta. Also, the equivalent nose radius applied by Gupta [10] and Sutton [8] is 18% smaller than the currently applied radius, which would have possibly reduced the shock-standoff distances, and therefore the radiation values, below those predicted by the present model. Gupta [10] does not present his predicted shock-standoff values, and so this cannot be confirmed. The reasonable agreement with Park's [17] prediction at 1643 s is noted. For the early nonequilibrium points presented in Fig. 11a, the present results provide the most consistent agreement with the data, excluding the results of Olynick et al. [16], which were discussed previously. A surprising result of Fig. 11a is the relatively close agreement between the NE VSL and E VSL models, even though the shock layer is in considerable chemical nonequilibrium. This is a result of the non-Boltzmann model suppressing the radiation from the regions of chemical nonequilibrium in the NE VSL flowfield, as shown in Fig. 9. Note that if the comparison between the NE and E VSL flowfields was made using a Boltzmann radiation model, the NE VSL prediction would be significantly larger than the E VSL prediction. Hence, if nonequilibrium chemistry is accounted for, a non-Boltzmann model must be applied.

The Fire II spectral radiometer data, which measured the intensity in the 2.2–4.1-eV spectral range, were presented and compared with past predictions in Sec. II. The results of the present radiation model, coupled with the NE VSL and E VSL models, are compared with this data in Fig. 12. The flight data are represented by two lines, representing the upper and lower limit of the data, which contained significant scatter. Decent agreement is seen for the NE VSL method throughout the entire trajectory, although it is slightly higher than the measurements for the early trajectory points. The radiation contained in this limited spectral range is due mostly to the N_2^+ first negative

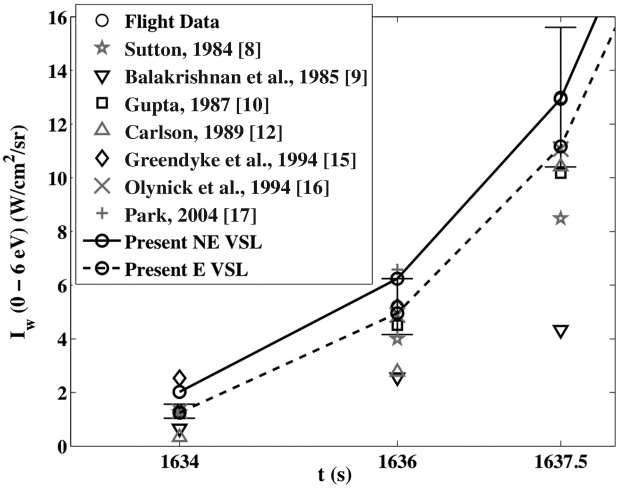

a) Early nonequilibrium trajectory points

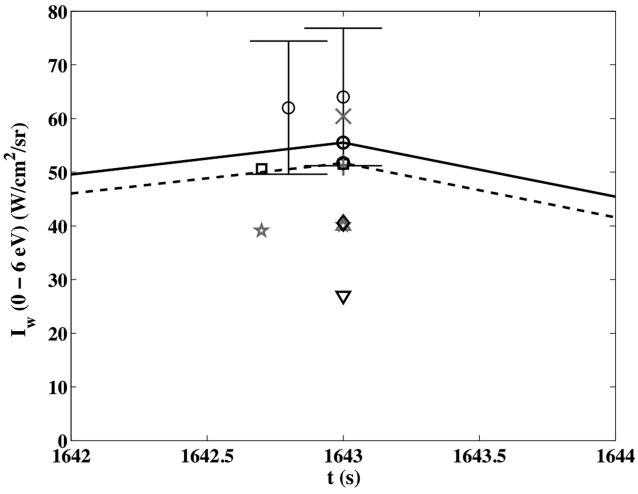

b) Peak heating trajectory points

Fig. 11 Comparison of the measured partial intensity (0–6 eV) with various predictions, including the coupled results of the present model.

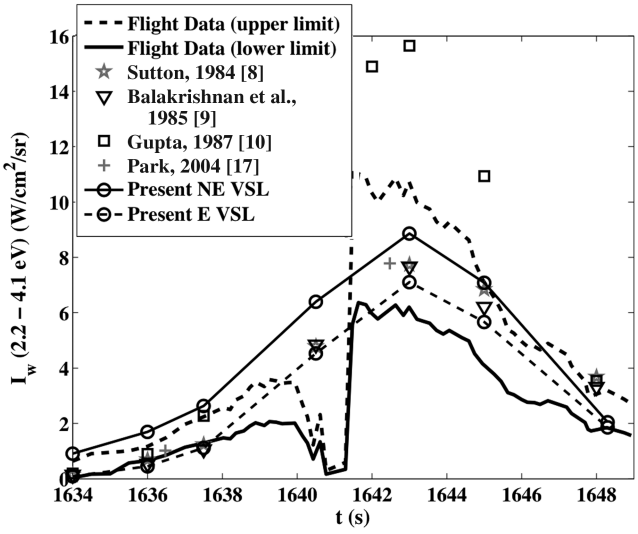

Fig. 12 Comparison of the partial intensity (2.2–4.1 eV) measured by the Fire II spectral radiometer with the present coupled results and previous predictions.

band system. For the 1634 to 1640-s points, this radiation is controlled significantly by the rates chosen by Johnston et al. [5,7] for the excitation of the $N_2^+(B)$ state. Note that both Sutton's [8] and Gupta's [10] values are larger than the present predictions for the peak

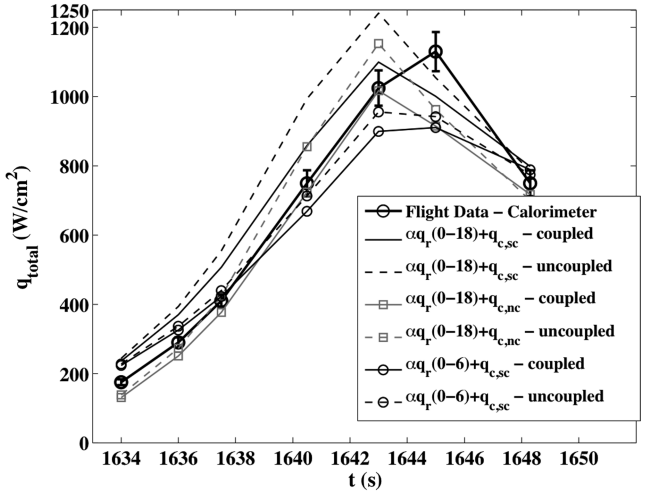

Fig. 13 Comparison of the present results, assuming a catalytic and noncatalytic wall, with the Fire II calorimeter data. These are coupled values from the nonequilibrium VSL flowfield.

heating points. Because Fig. 11b shows that the contribution from the 0–6-eV range in these studies is actually smaller than the present predictions, then the radiation from the 0–2.2-eV range must have been significantly underpredicted by Sutton and Gupta relative to the present model. This is likely a result of the increased line radiation in the 1–2-eV range resulting from the updated set of the atomic lines applied in the present model, and discussed by Johnston et al. [4].

The Fire II total calorimeter measurements presented by Cornette [3] contain the convective heating component along with the radiation absorbed by the beryllium calorimeter. This measured quantity, which will be labeled q_{total}, may be written as

$$q_{\text{total}} = q_c + \alpha q_r^- \tag{1}$$

where q_c is the convective heating and αq_r represents the radiation absorbed by the beryllium calorimeter. The absorbed radiation was obtained by multiplying the frequency-dependent radiative flux by the frequency-dependent absorptance (of polished beryllium) presented by Cauchon [2]. The two components of Eq. (1) are presented in Tables 3 and 4, with both the supercatalytic and noncatalytic values presented in each table. Figure 13 compares the supercatalytic and noncatalytic values for q_{total} with the flight data. For both the coupled and uncoupled *supercatalytic* cases, considering the flux from the 0–18 eV, a consistent overprediction of flight data is seen to exist at all trajectory points except the last two. Interestingly, the coupled *noncatalytic* case, considering the flux from the 0–18 eV, is seen to compare well for all trajectory points, except the 1645-s point. This comparison supports the argument that the beryllium surface of the calorimeter, at temperatures ranging from 600 to 1600 K, is closer to being noncatalytic than supercatalytic. Note that, as indicated by Fig. 3, the poor comparison at 1645 s is consistent with all previous theoretical predictions, and has not been explained. Although, due to the radiometer window reaching its melting point at this trajectory point, the radiometer measurement is not accurate enough to confirm the radiation prediction between 0 and 6 eV. Therefore, it is possible that some unknown radiation mechanism, not predicted by any previous study, contributed to the apparent shift of the peak heating point. Note that Sutton [8] showed that this shift was *not* due to the values used for the beryllium absorptance.

Because of the strong absorption of VUV radiation and the limitations of instrumentation windows to transmit in this spectral region, it is difficult to obtain quality data to assess the accuracy of theoretical predictions for VUV radiation. The Fire II calorimeter provides the best flight experimental data to infer the magnitude of VUV radiation, although it requires an assumption that the predictions for the convective heating and the radiation in the 0–6-eV spectral range are reasonably accurate. To indicate the influence of the VUV radiation in the present calculations, Fig. 13 presents the supercatalytic convective heating plus the absorbed radiative heating between 0 and 6 eV for both the coupled and uncoupled cases. The values presented here were taken from Tables 3 and 4, which means that the coupled cases considered the entire 0 to 18-eV radiation contribution while calculating the flowfield. It is seen that both the *uncoupled* and *coupled* values are below the flight data at the peak heating points.

Figure 13 implied the importance of the VUV radiation component by showing that it was required to achieve a good comparison between the calorimeter data and predictions, although a stronger conclusion may be made regarding the VUV radiation if the comparison between the radiometer data and predictions are included in the discussion. Table 5 achieves this by converting the intensity (between 0 and 6 eV) measured by radiometer [$I_{w,\text{meas}}(0–6)$] to the radiative flux absorbed by the calorimeter between 0 and 6 eV [$\alpha q^-_{r,\text{inferred}}(0–6)$], which is then subtracted along with the predicted convective heating from the actual calorimeter measurement $q_{\text{total,meas}}$, resulting in the radiative flux absorbed by the calorimeter between 6 and 18 eV [$aq^-_{r,\text{inferred}}(6–18)$]. The subscript "inferred" is used to indicate that the value is a result of the actual calorimeter and radiometer data, along with the predicted convective heating and the ratio between the predicted $\alpha q_r^-(0–6)$ and $I_w(0–6)$ values, labeled β in the table. Note that the predicted magnitude of the VUV radiation enters this analysis only indirectly through its influence on the coupled-radiation flowfield used to calculate q_c, $\alpha q^-_{r,\text{inferred}}(0–6)$, and $I_w(0–6)$. This makes the comparison between the inferred and

Table 5 Manipulation of the Fire II radiometer and calorimeter data with predictions to isolate the absorbed flux measured by the calorimeter in the 6–18-eV spectral range. The columns are defined below the table.

t, s	$I_{w,\text{meas}}(0–6)$[a]	β[b]	$\alpha q^-_{r,\text{inferred}}(0–6)$[c]	$\alpha q_r^-(0–6)$[d]	$q_{\text{total,meas}}$[e]	$\alpha q^-_{r,\text{inferred}}(0–18)$[f]	$\alpha q_r^-(0–18)$[g]	$\alpha q^-_{r,\text{inferred}}(6–18)$[h]	$\alpha q_r^-(6–18)$[i]
1634.0	1.3	3.1	4.1	6.33	175.0	−42.0 (64.0)	19.7	−46.1 (59.9)	13.4
1636.0	5.2	2.9	15.0	18.0	290.0	−18.0 (102)	62.4	−33.0 (87.0)	44.4
1637.5	13.0	2.8	35.9	35.6	410.0	23.0 (153)	120	−12.9 (117)	84.5
1640.5	35.0	2.6	91.1	106	750.0	187 (322)	296	95.8 (230)	190
1643.0	64.0	2.6	166.3	144	1025.0	269 (352)	344	103 (185)	200
1645.0	26.0	2.7	68.8	93.6	1130.0	313 (399)	184	244 (330)	90.4
1648.3	5.0	3.2	15.9	15.2	750.0	−24.0 (57)	24.6	−40.0 (41.1)	9.36

[a] $I_{w,\text{meas}}(0–6)$ = intensity measured by the radiometer (W/cm^2/sr).
[b] $\beta = \alpha q_r^-(0–6)/I_w(0–6)$, where both values are the predicted values.
[c] $\alpha q^-_{r,\text{inferred}}(0–6) = \beta I_{w,\text{meas}}(0–6)$, equals the $\alpha q_r^-(0–6)$ inferred by the radiometer measurement.
[d] $\alpha q_r^-(0–6)$ = predicted value listed in Table 4.
[e] $q_{\text{total,meas}}$ = calorimeter measurement = αq_r^-, $(0–18) + q_c$.
[f] $\alpha q^-_{r,\text{inferred}}(0–18) = q_{\text{total,meas}}$-$q_c$, where q_c is the predicted value. The values not in parentheses use the supercatalytic q_c, whereas values in parentheses use the noncatalytic q_c.
[g] $\alpha q_r^-(0–18)$ = predicted value listed in Table 4
[h] $\alpha q^-_{r,\text{inferred}}(6–18) = \alpha q^-_{r,\text{inferred}}(0–18)$-$\alpha q^-_{r,\text{inferred}}(0–6)$. The values not in parentheses use the supercatalytic value for $\alpha q^-_{r,\text{inferred}}(0–18)$, whereas values in parentheses use the noncatalytic value.
[i] $\alpha q_r^-(6–18)$ = predicted value listed in Table 4.

Table 6 Comparison of the predicted and experimentally inferred values, defined in Table 5, but now accounting for the shock-wave curvature by multiplying β, αq_r^-(0–6) and αq_r^-(6–18) by 0.85.

t, s	$\alpha q^-_{r,\text{inferred}}$(0–6)	αq_r^-(0–6)	$\alpha q^-_{r,\text{inferred}}$(6–18)	αq_r^-(6–18)
1634.0	3.4	5.4	−45.4 (60.5)	11.4
1636.0	12.7	15.3	−30.8 (89.2)	37.7
1637.5	30.5	30.3	−7.5 (122)	71.8
1640.5	77.5	90.0	109 (244)	161
1643.0	141	122	127 (210)	170
1645.0	58.6	79.6	254 (340)	76.8
1648.3	13.5	12.9	−37.5 (43.4)	7.9

predicted values in the last two columns of Table 5 meaningful. It is seen that, except for the 1643 and 1645-s points, the predicted values of the absorbed VUV radiation [αq_r^-(6–18)] fall between the $\alpha q^-_{r,\text{inferred}}$(6–18) values obtained using the supercatalytic (*not* in parentheses) and noncatalytic (*in* parentheses) q_c values. The negative $\alpha q^-_{r,\text{inferred}}$(0–18) and $\alpha q^-_{r,\text{inferred}}$(6–18) values in this table are a result of the $q_{\text{total,meas}}$ being lower than the predicted supercatalytic convective heating. The nonphysical nature of these negative values suggests that the heat shield for these cases is more accurately modeled with the noncatalytic assumption, which are shown in Table 5 to result in positive $\alpha q^-_{r,\text{inferred}}$(0–18) and $\alpha q^-_{r,\text{inferred}}$(6–18) values throughout the trajectory. The disagreement at 1645 s between the predicted and inferred values is not surprising, because it was not considered a "prime" data point by Cauchon [2] (although 1637.5 and 1640.5 were not either). On the other hand, the overprediction of αq_r^-(6–18) relative to $\alpha q^-_{r,\text{inferred}}$(6–18) (both the supercatalytic and noncatalytic value) at 1643 s is concerning because it is both a prime data point and the peak radiative heating point. A possible reason for this overprediction is that the tangent-slab approximation, applied for the radiation transport calculation, does not account for the shock-layer curvature. Past studies concerning the accuracy of the tangent-slab approximation have concluded that a detailed three-dimensional transport calculation produces a flux value about 10–20% lower than that predicted by the tangent-slab approximation [44]. Table 6 presents the values defined in Table 5, except now with both αq_r^-(0–6) and αq_r^-(6–18) multiplied by a factor of 0.85. Only the values that are influenced by this factor are presented in Table 6, with αq_r^-(0–6), αq_r^-(0–6), and $\alpha q^-_{r,\text{inferred}}$(0–6) each being reduced by 0.85 although $\alpha q^-_{r,\text{inferred}}$(6–18) is increased due to the reduction in $\alpha q^-_{r,\text{inferred}}$(0–6). With this adjustment, the 1643-s prediction for αq_r^-(6–18) now falls between the supercatalytic and noncatalytic inferred values. Note that the *intensity* predictions do not require the tangent-slab approximation, and so the previous conclusions regarding the radiometer data are not influenced by the inaccuracies of the tangent-slab assumption.

VII. Conclusions

The radiative heating for the Fire II flight experiment was studied using a radiation–flowfield coupled analysis consisting of a newly-developed thermochemical nonequilibrium VSL analysis and a non-Boltzmann radiation model. Past studies of the Fire II flight data were shown to provide a relatively wide scatter of values, none of which compared well with the flight data in both the nonequilibrium and equilibrium regions of the trajectory. The present analysis was shown to provide a good comparison with the data in both of these trajectory regions. The updated atomic-line and non-Boltzmann models are the reason for this good comparison relative to previous models. The influence of chemical equilibrium and the Boltzmann assumption of the electronic state populations were studied. These were shown to have only a small influence on the radiative heating at peak heating conditions and a relatively large influence at the earlier nonequilibrium conditions. The influence of radiation–flowfield coupling was shown to reduce the radiative heating by about 30%, also slightly reducing the convective heating. An analysis of the calorimeter data indicated that the present model provides reasonable values for the vacuum ultraviolet radiation, which is shown to be a significant contributor to the total radiation.

References

[1] Anderson, J. D., "An Engineering Survey of Radiating Shock Layers," *AIAA Journal*, Vol. 7, No. 9, 1969, pp. 1665–1675. doi:10.2514/3.5373

[2] Cauchon, D. L., "Radiative Heating Results from the Fire II Flight Experiment at a Reentry Velocity of 11.4 km/s," NASA TM X-1402, 1967.

[3] Cornette, E. S., "Forebody Temperature and Calorimeter Heating Rates Measured During Project Fire II Reentry at 11.35 km/s," NASA TM X-1305, 1966.

[4] Johnston, C. O., Hollis, B. R., and Sutton, K., "Spectrum Modeling for Air Shock-Layers at Lunar-Return Conditions," *Journal of Spacecraft and Rockets*, Vol. 45, No. 5, 2008, pp. 865–878.

[5] Johnston, C. O., Hollis, B. R., and Sutton, K., "Non-Boltzmann Modeling for Air Shock-Layers at Lunar Return Conditions," *Journal of Spacecraft and Rockets*, Vol. 45, No. 5, 2008, pp. 879–890.

[6] Johnston, C. O., Hollis, B. R., and Sutton, K., "Nonequilibrium Stagnation-Line Radiative Heating for Fire II," AIAA Paper 2007-3908, 2007.

[7] Johnston, C. O., "Nonequilibrium Shock-Layer Radiative Heating for Earth and Titan Entry," Ph.D. Dissertation, Virginia Polytechnic Inst. and State Univ., Blacksburg, VA, Nov. 2006.

[8] Sutton, K., "Air Radiation Revisited," AIAA Paper 84-1733, 1984.

[9] Balakrishnan, A., Park, C., and Green, M. J., "Radiative Viscous-Shock-Layer Analysis of Fire, Apollo, and PAET Flight Data," AIAA Paper 85-1064, 1985.

[10] Gupta, R. N., "Navier–Stokes and Viscous Shock-Layer Solutions for Radiating Hypersonic Flows," AIAA Paper 87-1576, 1987.

[11] Bird, G. A., "Nonequilibrium Radiation During Re-Entry at 10 km/s," AIAA Paper 87-1543, 1987.

[12] Carlson, L. A., "Approximations for Hypervelocity Nonequilibrium Radiating, Reacting, and Conducting Stagnation Regions," *Journal of Thermophysics and Heat Transfer*, Vol. 3, No. 4, 1989, pp. 380–388. doi:10.2514/3.28764

[13] Park, C., "Assessment of Two-Temperature Kinetic Model for Ionizing Air," *Journal of Thermophysics and Heat Transfer*, Vol. 3, No. 3, July 1989, pp. 233–244. doi:10.2514/3.28771

[14] Gally, T. A., "Development of Engineering Methods for Non-equilibrium Radiative Phenomena about Aeroassisted Entry Vehicles, Ph.D. Dissertation, Texas A&M Univ., College Station, TX, 1992.

[15] Greendyke, R. B., and Hartung, L. C., "Convective and Radiative Heat Transfer Analysis for the Fire II Forebody," *Journal of Spacecraft and Rockets*, Vol. 31, No. 6, 1994, pp. 986–992. doi:10.2514/3.26548

[16] Olynick, D. R., Henline, W. D., Chambers, L. H., and Candler, G. V., "Comparisons of Coupled Radiative Navier–Stokes Flow Solutions with the Project Fire II Flight Data," AIAA Paper 94-1955, 1994.

[17] Park, C., "Stagnation-Point Radiation for Apollo 4," *Journal of Thermophysics and Heat Transfer*, Vol. 18, No. 3, 2004, pp. 349–357. doi:10.2514/1.6527

[18] Greendyke, R. B., and Hartung, L. C., "Approximate Method for the Calculation of Nonequilibrium Radiative Heat Transfer," *Journal of Spacecraft and Rockets*, Vol. 28, No. 2, 1991, pp. 165–171. doi:10.2514/3.26225

[19] Hartung, L. C., Mitcheltree, R. A., and Gnoffo, P. A., "Stagnation Point Nonequilibrium Radiative Heating and the Influence of Energy Exchange Models," *Journal of Thermophysics and Heat Transfer*, Vol. 6, No. 3, 1992, pp. 412–418. doi:10.2514/3.376

[20] Park, C., "Problems of Rate Chemistry in the Flight Regimes of Aeroassisted Orbital Transfer Vehicles," AIAA 84-1730, 1984.

[21] Park, C., "Assessment of Two-Temperature Kinetic Model for Dissociating and Weakly Ionizing Nitrogen," *Journal of Thermophysics and Heat Transfer*, Vol. 2, No. 1, July 1988, pp. 8–16. doi:10.2514/3.55

[22] Park, C., "Assessment of Two-Temperature Kinetic Model for Ionizing Air," *Journal of Thermophysics and Heat Transfer*, Vol. 3, No. 3, July 1989, pp. 233–244. doi:10.2514/3.28771

[23] Cauchon, D. L., Mckee, C. W., and Cornette, E. S., "Spectral Measurements of Gas-Cap Radiation During Project Fire Flight Experiment at Reentry Velocities Near 11.4 km/s," NASA TM X-1389, 1967.

[24] Hartung, L. C., "Development of a Nonequilibrium Radiative Heating Prediction Method for Coupled Flowfield Solutions," *Journal of Thermophysics and Heat Transfer*, Vol. 6, No. 4, 1992, pp. 618–625. doi:10.2514/3.11542

[25] Greendyke, R. B., "Parametric Analysis of Radiative Structure in Aerobrake Shock Layers," *Journal of Spacecraft and Rockets*, Vol. 30, No. 1, 1993, pp. 51–57. doi:10.2514/3.25470

[26] Davis, R. T., "Numerical Solution of the Hypersonic Viscous Shock-Layer Equations," *AIAA Journal*, Vol. 8, No. 5, 1970, pp. 843–851. doi:10.2514/3.5776

[27] Gnoffo, P. A., Gupta, R. N., and Shinn, J. L., "Conservation Equations and Physical Models for Hypersonic Air Flows in Thermal and Chemical Nonequilibrium," NASA TP-2867, 1989.

[28] Park, C., "Review of Chemical-Kinetic Problems of Future NASA Missions, 1: Earth Entries," *Journal of Thermophysics and Heat Transfer*, Vol. 7, No. 3, 1993, pp. 385–398. doi:10.2514/3.431

[29] Mcbride, B. J., Zehe, M. J., and Gordon, S., "NASA Glenn Coefficients for Calculating Thermodynamic Properties of Individual Species," NASA TP 2002-211556, Sept. 2002.

[30] Gupta, R. N., Yos, J. M., Thompson, R. A., and Lee, K. P., "A Review of Reaction Rates and Thermodynamic and Transport Properties for an 11-Species Air Model for Chemical and Thermal Nonequilibrium Calculations to 30,000 K," NASA RP-1232, 1990.

[31] Sutton, K., and Gnoffo, P. A., "Multi-Component Diffusion with Application to Computational Aerothermodynamics," AIAA Paper 98-2575, 1998.

[32] Ralchenko, Yu, Jou, F.-C., Kelleher, D. E., Kramida, A. E., Musgrove, A., Reader, J., Wiese, W. L., and Olsen, K., "NIST Atomic Spectra Database, Version 3.1.0," National Inst. of Standards and Technology (NIST) Physics Lab., http://physics.nist.gov/PhysRefData/ASD/index.html, July 2006 [retrieved 3 Sept. 2006].

[33] *The Opacity Project*, Vol. 1, Taylor and Francis Philadelphia, 1995.

[34] Cunto, W., Mendoza, C., Ochsenbein, F., and Zeippen, C. J., "TOPbase at the CDS," *Astronomy and Astrophysics*, Vol. 275, 1993, pp. L5–L8, http://vizier.u-strasbg.fr/topbase/topbase.html [retrieved 3 Sept. 2006].

[35] Soon, W. H., and Kunc, J. A., "Nitrogen Plasma Continuum Emission Associated with N-(3P) and N-(1D) Ions," *Physical Review A*, Vol. 41, No. 8, 1990, pp. 4531–4533. doi:10.1103/PhysRevA.41.4531

[36] Chauveau, S., Deron, C., Perrin, M. Y., Riviere, P., and Soufiani, A., "Radiative Transfer in LTE Air Plasmas for Temperatures up to 15,000 K," *Journal of Quantitative Spectroscopy and Radiative Transfer*, Vol. 77, No. 2, 2003, pp. 113–130. doi:10.1016/S0022-4073(02)00080-8

[37] Chambers, L. H., "Predicting Radiative Heat Transfer in Thermochemical Nonequilibrium Flow Fields," NASA TM-4564, 1994.

[38] Laux, C. O., "Optical Diagnostics and Radiative Emission of Air Plasmas," High Temperature Gas Dynamics Lab., Mechanical Engineering Dept., Stanford Univ., Rept. T-288, Stanford, CA, 1993.

[39] Whang, T. J., Guoxing, Z., Stwalley, W. C., and Wu, C. Y. R., "Franck-Condon Factors of the $\cdots$. Transitions of N_2," *Journal of Quantitative Spectroscopy and Radiative Transfer*, Vol. 55, No. 3, 1996, pp. 335–344. doi:10.1016/0022-4073(95)00169-7

[40] Stahel, D., Leoni, M., and Dresslar, K., "Nonadiabatic Representations of the $^1\Sigma_u$ and $^1\Pi_u$ States of the N_2 Molecule," *Journal of Chemical Physics*, Vol. 79, No. 6, Sept. 1983, pp. 2541–2558. doi:10.1063/1.446166

[41] Chauveau, S., Perrin, M. Y., Riviere, P., and Soufiani, A., "Contributions of Diatomic Molecular Electronic Systems to Heated Air Radiation," *Journal of Quantitative Spectroscopy and Radiative Transfer*, Vol. 72, No. 4, 2002, pp. 503–530. doi:10.1016/S0022-4073(01)00141-8

[42] Park, C., "Radiation Enhancement by Nonequilibrium in Earth's Atmosphere," *Journal of Spacecraft and Rockets*, Vol. 22, No. 1, pp. 27–36. doi:10.2514/3.257061985.

[43] Hash, D., Olejniczak, J., Wright, M., Prabhu, D., Pulsonetti, M., Hollis, B., Gnoffo, P., Barhardt, M., Nompelis, I., and Candler, G., "Fire II Calculations for Hypersonic Nonequilibrium Aerothermodynamics Code Verification: DPLR, LAURA, and US3D," AIAA Paper 2007-605, Jan. 2007.

[44] Hartung, L. C., and Hassan, H. A., "Radiation Transport Around Axisymmetric Blunt Body Vehicles Using a Modified Differential Approximation," *Journal of Thermophysics and Heat Transfer*, Vol. 7, No. 2, 1993, pp. 220–227. doi:10.2514/3.410

G. Palmer
Associate Editor